Supplemental Data

Local Cortical Tension by Myosin II

Guides 3D Endothelial Cell Branching

Robert S. Fischer, Margaret Gardel, Xuefei Ma, Robert Adelstein, and Clare M. Waterman

Supplemental Experimental Procedures

Reagents. GFP-β-actin mice were a gift from Andrew Matus (Friedrich Miescher Institute, Basel, Switzerland). Tie2-driven GFP *danio rerio* embryos were a gift from Konstantin Stoletov and Richard Klemke (University of California, San Diego, CA). GFP-myosin heavy chain IIB mice were generated as previously described [1]. Blebbistatin, Y-27632, and ML-7, H1152, γ-secretase inhibitors DAPT and L-685,486, and Rac inhibitor NSC23766 , were obtained from Sigma (St. Louis, MO) and Calbiochem (San Diego, CA) and cell permeable C3-exoenzyme was obtained from Cytoskeleton Inc (Denver, CO) Polyclonal antibodies to myosin IIA have been previously described[2]. Antibodies to phosphomyosin light chain 2 were obtained from Cell Signaling Technology (Danvers, MA), VEGFR1 from Abcam (Cambridge, MA) smooth muscle caldesmon from Sigma (St. Louis, MO) and rat anti-mouse CD31 and Alexa 488-conjugated isolectin *Griffonia simplicifolia* (GS lectin, I-21413) from Invitrogen, (San Diego, CA). Rat tail collagen I was obtained from Gibco/Invitrogen (Carlsbad, CA), and collagen IV was obtained from Trevigen (Gaithersburg, MD).

3D collagen matrix EC cultures. Primary aortic slice cultures were established from mice donors (either wild type, GFP-myosin IIA, or GFP β-actin, on mixed BL6/SVJ backgrounds) essentially as described [3]. Mice were euthanized and blood was collected by cardiac puncture. Briefly, aortas were removed and extensively surgically cleaned to remove adipose tissue, cut longitudinally and then horizontally to create tissue slices. Slices were embedded into 1.6 mg/ml

rat tail collagen in MEM, and allowed to polymerize into fibrils at 37°C in 35 mm coverglass-bottomed dishes (Ma-Tek, Ashland, MA) for at least 6 hours to form a matrix ~400 to 700 μm thick before being overlaid with either EGM-MV (Lonza, Basel, Switzerland) or MCDB plus 3% mouse serum. The concentrations of polymerized native collagen I used produces a matrix with a viscoelastic modulus of less than 200 Pa ([4], and data not shown). For live cell microscopy, immediately prior to imaging, matrices were removed from dishes to mount in Rose chambers to eliminate the possibility of imaging cells with contact to the coverglass. Cells in aortic slice cultures were verified to be of endothelial origin by positive staining with GS lectin or immunostaining for CD31 and VEGFR1 (Supplemental Figure 1), and negative immmunostaining for smooth muscle caldesmon (data not shown).

Collagen/PA/glass sandwich gel preparation and cultures. Polyacrylamide (PA) substrates bound to glass coverslips were prepared as previously described [5] except that they were additionally embedded with Tetraspec Beads (Invitrogen, Carlsbad, CA) to visualize the PA gel. PA gel viscoelastic moduli for various bisacrylamide and acrylamide concentrations were based on recipes and values previously described [6]. PA gels were activated for crosslinking to collagen with UV using sulfo-SANPAH (Pierce, Rockford, IL), and inverted onto unpolymerized, neutralized rat tail collagen at 1.6 mg/ml. Crosslinking proceeded for 4 hours at 4^{o}C, then collagen fibrils were polymerized at 37^{o}C in a humidified chamber for at least 6 hours followed by extensive rinsing with warm culture media. Aortic slices were prepared as above, and endothelial (inner) sides placed on the collagen matrix, and held in place using either dialysis tubing or by polymerizing additional 1.6 mg/ml rat tail collagen I (in MEM) on top of the tissue slice. Cells migrating on collagen that was directly coupled to the PA were found as the bottommost layer of cells, as they cannot invade the biologically inert PA gel.

For 2D collagen/PA cultures, PA gels were prepared as above. Collagen I (1.6 mg/ml) was covalently coupled to the PA gel via UV-activated sulfo-SANPAH at 4^{o}C, and gels were

rinsed three times in 15 mM acetic acid to remove uncrosslinked collagen, then 10 times in PBS, then twice in culture media. Mouse ECs were digested out of 3D collagen matrices from standard aortic ring cultures using 0.25% collagenase in serum free media, and replated onto 2D collagen/PA substrates. Cells were imaged on these substrates 12-40 hours post-plating.

Immunofluorescence of 3D collagen matrix cultures. Collagen matrices containing mouse ECs were removed from dishes, cut into smaller pieces, and placed into 12 well dishes. Pieces of maxtix were fixed in 3% paraformaldehyde in CB buffer (10mM MES pH 6.1, 138mM KCl, 3mM MgCl2, 2mM EGTA) with 0.1% Triton X-100 for 30 minutes at room temperature, rinsed in CB with 0.2% Triton X-100 for 30 minutes. We found that even with paraformaldehyde fixation, autofluorescence of the collagen matrix was reduced by two 10 minute washes in CB with 0.5 mg/ml $NaBH_4$. Gels were then blocked in CB with 2% bovine serum albumin, 1% goat serum, 0.2% Triton X-100 overnight at 4C. Matrix pieces were then stained with primary antibodies overnight in blocking buffer, rinsed in CB with 0.2% Triton extensively at room temperature, followed by staining with fluorescent secondary antibodies and/or phalloidin/phallacidin in blocking buffer for 4-6 hours at 4C. Matrix pieces were then rinsed overnight at 4C in CB buffer, and mounted for microscopy. For phosphomyosin/F-actin ratio measurements, cells in stiff or soft collagen/PA/glass sandwich gels were fixed and stained as above using fluorescent phalloidin and primary antibody to phosphomyosin light chain 2 followed by fluorescent anti-mouse secondary antibody.

Microscopy. 3D imaging of fixed and stained cells was performed using a Zeiss LSM 510 equipped with a 1.1 NA 63X water immersion objective lens and KrAr and HeNe lasers. Each confocal plane was the result of two-fold Kalman averages. Fluorescence channels were acquired sequentially every plane, and Z-stacks were acquired with image planes taken every 0.3 μm. Combined channel Z-stacks were then used to create maximum intensity projections

(see below). Phase-contrast microscopy of ECs in 3D collagen matrices was performed using a Nikon TE300 equipped with 20x 0.5 NA LWD or 40x 0.6NA ELWD phase contrast objective lenses, a 0.55 NA LWD phase contrast condenser, a linear encoded X,Y,Z robotic stage (ASI Technologies, Montgomeryville, PA) and an electronic shutter (Uniblitz; Rochester, NY) for transmitted illumination. 12 bit images were acquired using an interline transfer cooled CCD (Orca II, Hamamatsu, Bridgewater, NJ) and microscope control was provided by MetaMorph software (Molecular Devices, Sunnyvale, CA). For local application of blebbistatin, this microscope was equipped with a micromanipulator and pressure injection system (Injectman, Eppendorf, Westbury, NY). Spinning disk confocal microscopy and FRAP were performed using a 60x 1.2 NA water immersion objective lens on a Nikon TE2000 equipped with Perfect Focus System, a mechanical shutter (Smart shutter, Sutter Instruments; Novato, CA) for transmitted illumination, a linear encoded X, Y, Z robotic stage with a piezo-driven Z-axis top-plate (ASI Technologies, Montgomeryville, PA) and a Yokogawa CSU-X spinning disk confocal scan head equipped with a multi-bandpass dichromatic mirror (Semrock; Rochester, NY) and bandpass filters (Chroma; Rockingham, VT), selected with an electronic filterwheel, for GFP and Texas red excitation and emission. 561 and 488 nm laser illumination was provided by a custom-built laser combiner module (modification of LMM-3, Spectral Applied Research; Richmond Hill, Ontario, Canada) containing 500mW solid state lasers (488 nm: Coherent; 561 nm: MPB Communications; Montreal, Quebec) that were shuttered with electronic mechanical shutters and attenuated and/or directed to one of two fiber-coupled output ports with an AOTF (Neos Technologies, Melbourne, FL). Laser output for directing illumination to the confocal scanhead was via a single-mode optical fiber (Oz Optics, Ottawa, Ontario, Canada). Laser output for FRAP was directed via a multimode fiber bundle to an electronically controlled micromirror device in the field plane of an epi-illuminator for creating defined photobleach areas (Mosaic, Photonic Instruments, St. Charles, IL). 14 Bit Images were acquired with an interline-

transfer cooled CCD (HQ2, Photometrics, Tucson, AZ) and microscope control was provided by MetaMorph software.

Image Acquisition

Intravital imaging of zebrafish embryos was perfomed essentially as previously described [8]. Briefly, 22-26 hour post-fertilization embryos were dechorinated manually in embryo medium (10% Hanks Buffered saline, 2 mM $CaCl_2$, 3 mM $MgCl_2$) and placed in embryo medium with 0.005% tricaine methanesulfonate to anesthetize them. Embryos were positioned against the coverglass in glass-bottomed tissue culture dishes (MatTek, Ashland, MA). Spinning disc confocal images were acquired at 0.4 μm z intervals over 7-10 μm z-distance, each such z-stack was acquired once every 10 seconds. To minimize online movie content size, frame rates of movies have been decreased by removing alternate frames, and best focus z-planes are shown.

For phase images of aortic slice ECs in 3D collagen matrix or collagen/PA/glass sandwich gels, cells were maintained in gels with tissue culture media containing 20 mM HEPES pH 7.4 in Rose chambers at 37C on the microscope stage using an air-stream incubator (NevTek). Cells were imaged every 1-2 minutes for 4-6 hours. For samples with pharmacological inhibitors, cells were incubated with inhibitor for 1 hour at 37C prior to the start of image acquisition. For single focal plane spinning disk confocal imaging of GFP-myosin IIB, ECs embedded in collagen matrices were imaged every 30 seconds. For FRAP analyses, ECs in soft or stiff collagen/PA/glass sandwich gels were imaged for 5 frames every 5 seconds prior to photobleaching. Photobleaching was accomplished by delivering 300 mW of 488 laser light to the Mosaic micromirror array, resulting in bleach times of 1.2 seconds or less. Post-bleach images were then acquired every 0.7 seconds immediately after photobleaching for 20 seconds, then every 3 seconds for the next 2 minutes (see analysis section below). FRAP regions were chosen either within the cell cortex or in the cell cytoplasm and bleached simultaneously.

Data Analysis.

3D reconstructions and movies of rotation of these 3D reconstructions were created from maximum intensity projections using Metamorph software. To quantify branches per cell, 2D maximum intensity projections of 3D stacks were created such that all branches of the cells within the field were contained within the image. Branches were counted as number of branch tips observed per cell nucleus, and at least 4 image fields containing at least 2 cells each for each sample were counted. For quantification of branch tips in 2D cultures, cells with only a single flat lamella were counted as zero branches per cell. A divided lamella with a lateral cell edge convexity of less than 90 degrees and larger than 10 microns extension was counted as a branched extension.

For quantification of cell speed and persistence distance, individual nuclei of at least 40 cells for each condition were tracked using the “track points” function in Metamorph software. Cells with predominantly lateral migration during the time of imaging were chosen, and cells which moved out of focus during observation were not included. For simplicity, no effort was made to correct for tangential errors in distance to Z movement. However, even for cells migrating at a 30 degree angle to horizontal, the error in measuring lateral distance would be 1-1/cos(θ), or approximately 15%. i.e, much less than the cell to cell variation. Therefore, the contribution of this potential error was assumed to be the same for all cells in all experimental conditions. Cell migration speed (S) and persistence (P) were calculated using a persistent random walk equation $\langle d^2(t)\rangle = 2S^2P[t-P(1-e^{-t/p})]$ as described previously [9]. Migration speed of individual cells was estimated from double reciprocal plots of the square root of $\langle d^2(t)\rangle$ against t as 1/slope, using distance to origin over time to estimate $\langle d^2(t)\rangle$. Cell persistence was estimated as (slope/6)*Y-intercept, and then the persistence distance was calculated as S*P. These data were then analyzed using Excel (Microsoft) and Analyze-It (www.analyse-it.com) softwares to generate box and whisker plots and statistical comparison.

For protrusion dynamics, individual protrusions and retractions were tracked by hand using “track points” in Metamorph. Lateral protrusions were viewed using phase contrast optics, and protrusions which moved out of focus or began prior to imaging were not counted. For protrusion initiation frequency, protrusion initiation events greater than 5 μm in length away from the cell body (using a movable circular image caliper 5 μm in diameter) were counted and labeled frame by frame manually for each cell; for every sample at least 15 cells were counted over a minimum of 2 hours. Protrusion and retraction velocities, protrusion initiation frequency per cell and protrusion persistence times were then calculated using Excel (Microsoft) and Analyze-It softwares. For statistical analysis of protrusions induced by local blebbistatin application, we scored each experiment with a binary count (protruded, did not protrude) and performed ANOVA analysis using Microsoft Excel.

For phosphomyosin/F-actin ratio measurements, images were acquired using Metamorph as above using consistent imaging parameters between preps, and background was subtracted using equal areas of images containing no cells. Matching images were used to calculate ratios and cell areas were determined using parallel threshold parameters. The intensity per area was quantified and then tabulated and graphed in Excel. Data represent at least 25 cells per category.

For FRAP, the intensity in regions of bleached cell cortex, unbleached cell cortex and background area in image series was quantified using Metamorph. Relative recovery curves with imaging bleach correction were fit to double exponential recovery kinetics, and $t_{1/2}$ and total percent recoveries calculated using these fitted curves.

Supplemental References

1. Bao, J., Ma, X., Liu, C., and Adelstein, R.S. (2007). Replacement of nonmuscle myosin II-B with II-A rescues brain but not cardiac defects in mice. J Biol Chem *282*, 22102-22111.
2. Rochlin, M.W., Itoh, K., Adelstein, R.S., and Bridgman, P.C. (1995). Localization of myosin II A and B isoforms in cultured neurons. J Cell Sci *108 (Pt 12)*, 3661-3670.
3. Zhu, W.H., Iurlaro, M., MacIntyre, A., Fogel, E., and Nicosia, R.F. (2003). The mouse aorta model: influence of genetic background and aging on bFGF- and VEGF-induced angiogenic sprouting. Angiogenesis *6*, 193-199.
4. Forgacs, G., Newman, S.A., Hinner, B., Maier, C.W., and Sackmann, E. (2003). Assembly of collagen matrices as a phase transition revealed by structural and rheologic studies. Biophys J *84*, 1272-1280.
5. Lo, C.M., Wang, H.B., Dembo, M., and Wang, Y.L. (2000). Cell movement is guided by the rigidity of the substrate. Biophys J *79*, 144-152.
6. Johnson, K.R., Leight, J.L., and Weaver, V.M. (2007). Demystifying the effects of a three-dimensional microenvironment in tissue morphogenesis. Methods Cell Biol *83*, 547-583.
7. Dorrell, M.I., Aguilar, E., and Friedlander, M. (2002). Retinal vascular development is mediated by endothelial filopodia, a preexisting astrocytic template and specific R-cadherin adhesion. Invest Ophthalmol Vis Sci *43*, 3500-3510.
8. Lawson, N.D., and Weinstein, B.M. (2002). In vivo imaging of embryonic vascular development using transgenic zebrafish. Dev Biol *248*, 307-318.
9. Lo, C.M., Buxton, D.B., Chua, G.C., Dembo, M., Adelstein, R.S., and Wang, Y.L. (2004). Nonmuscle myosin IIb is involved in the guidance of fibroblast migration. Mol Biol Cell *15*, 982-989.

Supplemental Figures

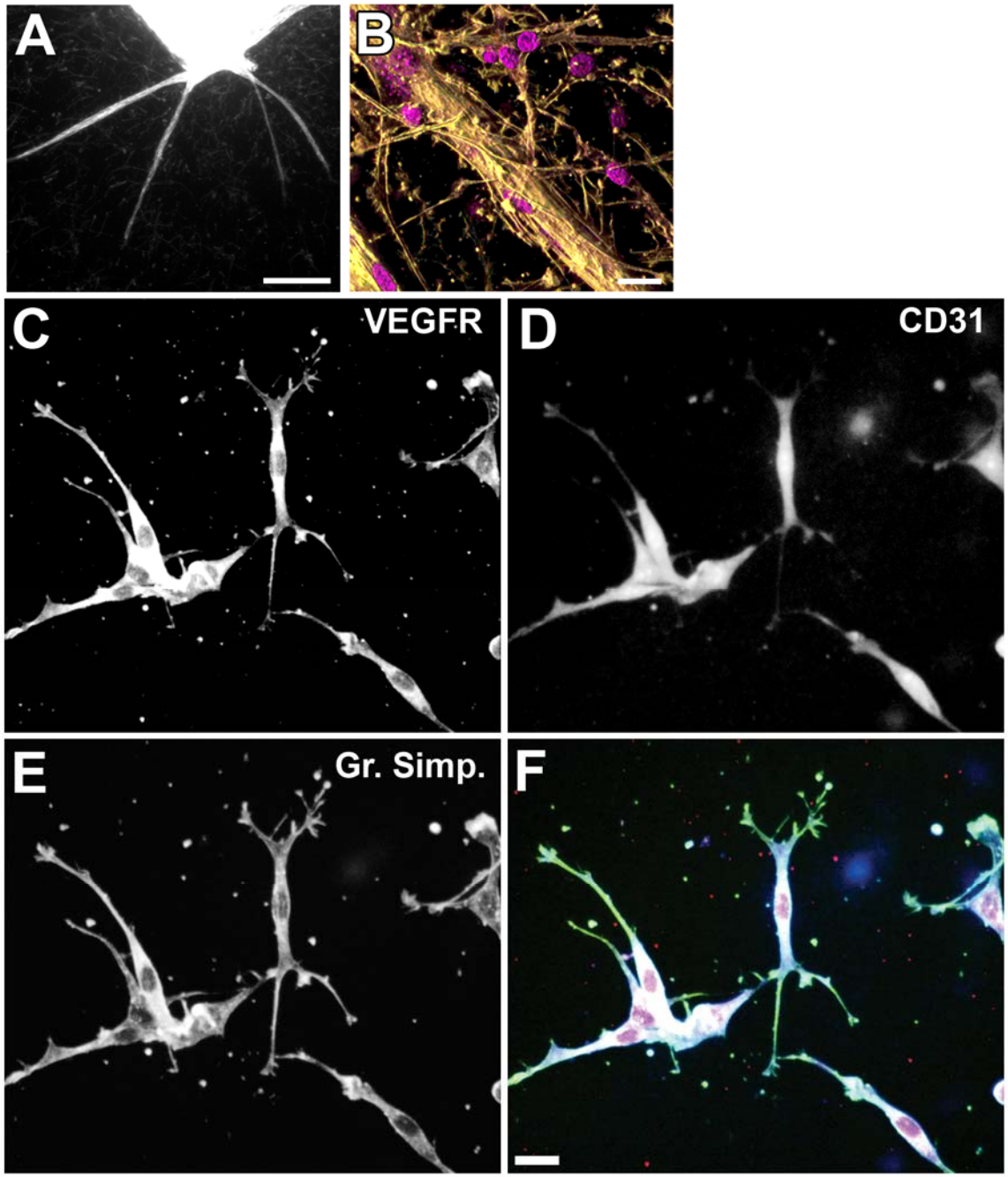

Figure S1 (A) Low magnification epifluoresence image of endothelial tubes extending from mouse aortic slice stained with fluorescent phalloidin in 3D collagen matrices. Bar equals 0.6

mm (B) 3D reconstruction of mouse endothelial tubes formed in 3D collagen cultures. Violet shows DAPI stained nuclei, yellow indicates phalloidin-stained F-actin. Bar equals 12 μm. (C-F) Single cells in 3D collagen matrix cultures of mouse aorta continue to express endothelial markers. Cells were stained in matrices in situ as described in Methods, using antibodies to (E) VEGF receceptor 1 (VEGFR), (F) CD31/PECAM (CD31) and (H) endothelial specific lectin *Griffonia simplicifolia* (Gr. Simp.). Bar equals12 microns.

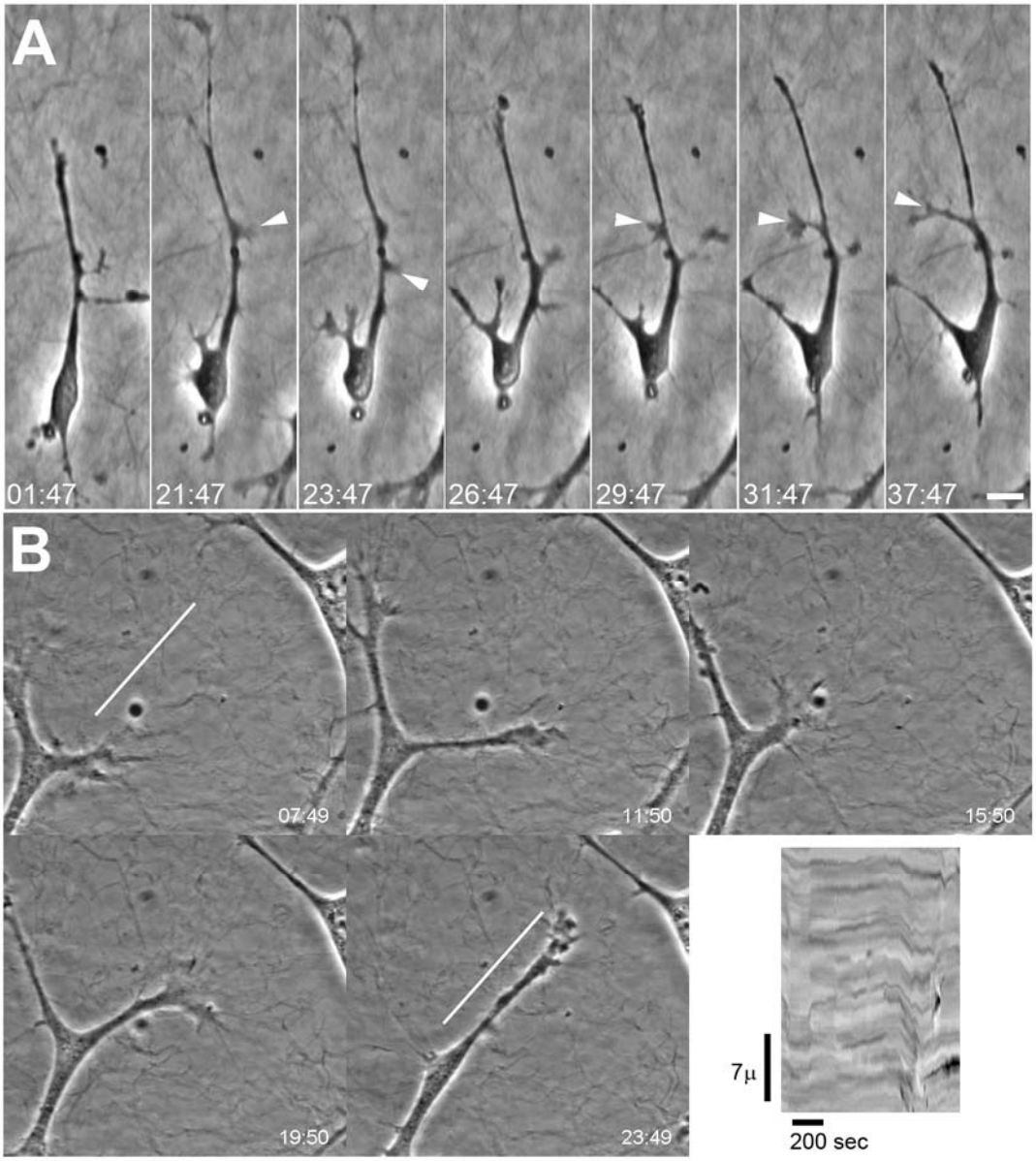

Figure S2. (A) In 3D collagen matrix, mouse aortic EC pseudopods initiate as lamellipodial protrusions along the cell body or sides of existing branches. Images are from a time-lapse phase-contrast movie (Supplemental Video 3). Arrowheads indicate lamellipodial tips. Note that many initial protrusions (frame 3, left-pointing arrowhead) are rapidly retracted, while others successfully extend to form pseudopodial branches (frames 5-7 right pointing arrowheads). Bar=10μm. (B) Collagen matrix is deformed by EC pseudopodia (Supplemental movie 5). Shown are frames from a time-lapse phase-contrast movie showing local deformation of the

collagen matrix as EC pseudopodia move through it. Bottom right panel shows a kymograph taken along the line shown in the first and last panels of the time-lapse. Note that pseudopodia are tipped by both small lamellipodia and surface blebs during forward progress, and that the collagen fibers undergo centripetal contraction at the branch tip, but are pulled uniformly along the branch length as well (kymograph). Time in (B) shown in min:s. Bar= (A, B) 10 μm.

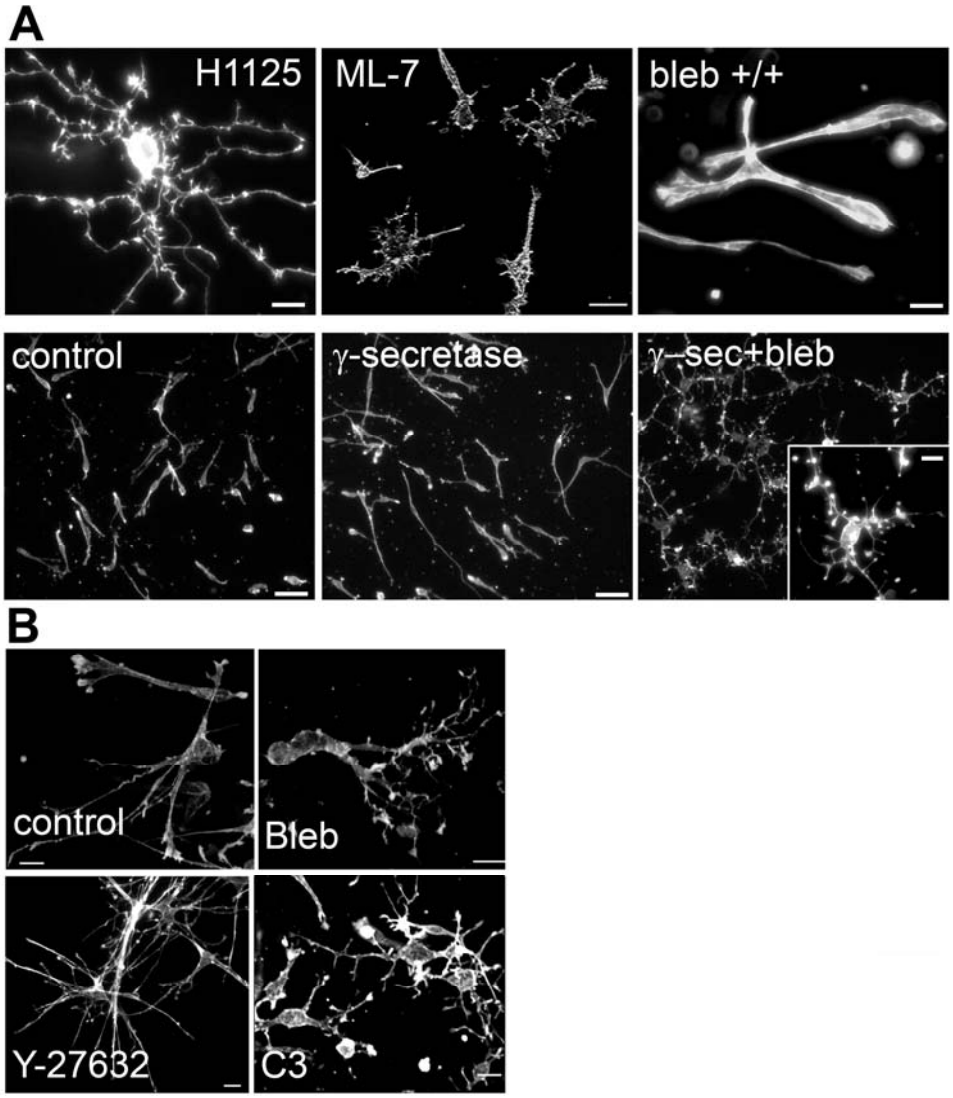

Figure S3. Effects of pharmacological agents on mouse EC pseudopodia morphology in 3D collagen matrices. ECs cultured in 3D collagen matrices for 5 days were incubated in various agents for 12 hours. Cells were then fixed and stained *in situ* with fluorescent phalloidin as described in methods. (A) The ROCK inhibitor H1152 and the myosin light chain kinase inhibitor ML-7 were incubated at 2 μM, and the +/+ enantiomer of blebbistatin was incubated at 50 μM. The γ-secretase inhibitor, (L-685,486; similar results were obtained with DAPT, not shown) was used at 1 μM. Blebbistatin (bleb) was used at 30 μM. Bars in top row and inset are 12 microns, bottom row bars are 30 microns. (B) Mouse ECs in 3D matrices stained as in (A); exposed to

vehicle alone, 30μM blebbistatin, 10μM Y-27632, or 2μM cell permeable C3-exoenzyme. Bars equal 9 μm.

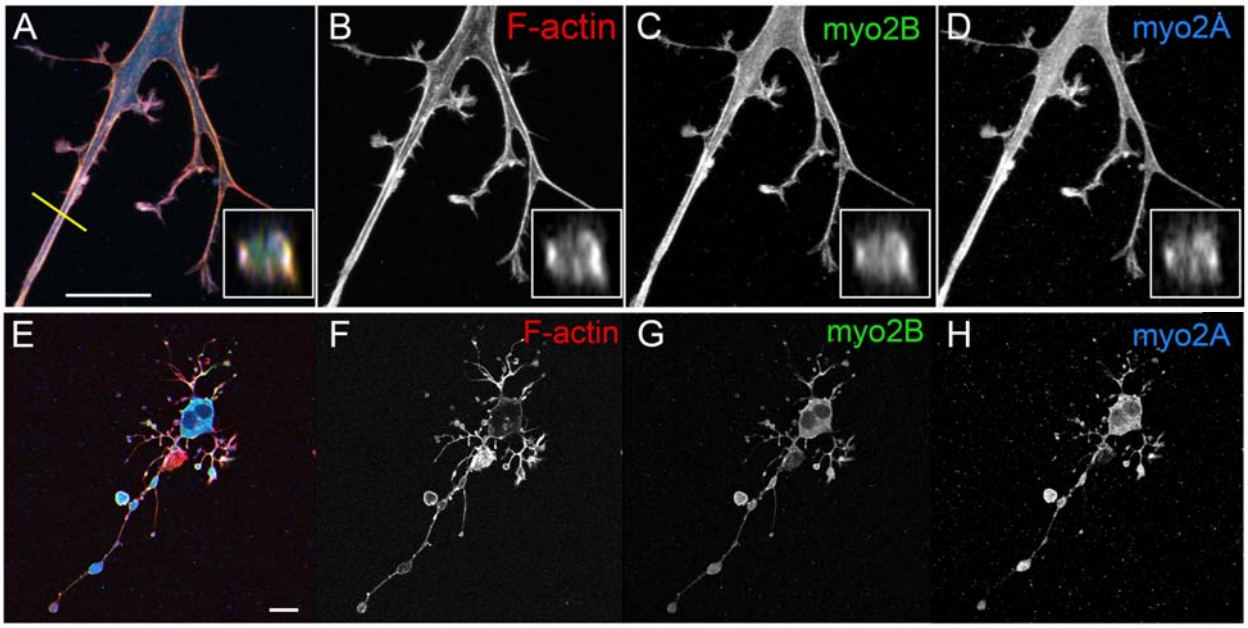

Figure S4. Localization of myosin IIA and IIB at the cortex of control (A-D) and blebbistatin treated (E-H) mouse aortic ECs in 3D collagen matrices. Maximal projections of 3D reconstructions of confocal optical sections of an EC, showing bodipy phallacidin staining of F-actin (B), GFP-myosin IIB (C), and immunostaining of myosin IIA (D). Bar equals (A-D) 7 μm, (E-H) 15μm. Note that in the presence of blebbistatin, myosin IIA and B accumulate at the cortex of blebs, and lamellipodia still persist at the tips and sides of pseudopodia.

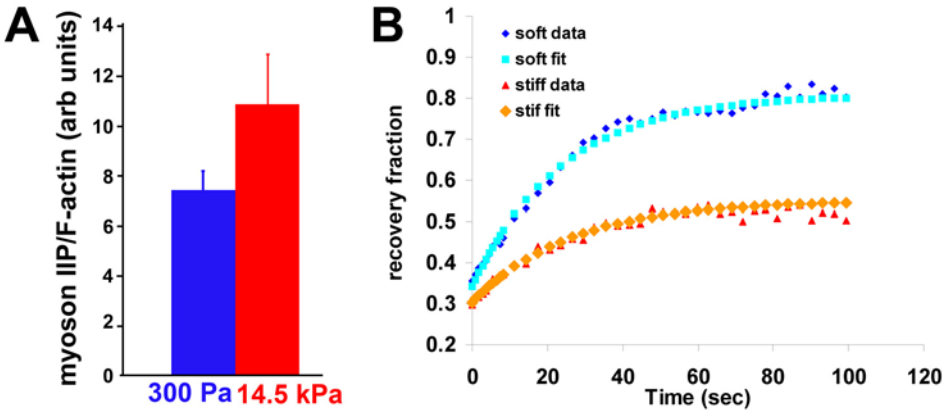

Figure S5. Cortical myosin II regulation in ECs on soft versus stiff sandwich substrates. (A) Quantification of fluorescence intensity ratio of myoP: F-actin for ECs in soft (300 Pa, top row) versus stiff (14.5kPa, bottom row) collagen/PA/glass sandwich gels. Phosphomyosin light chain 2 in cells on soft versus stiff sandwich substrates. Cells in soft (300 Pa) or stiff (14.5 kPa) sandwich gels were fixed and stained as described in Methods, using fluorescent phalloidin and a monoclonal antibody to phosphoserine 19 of myosin light chain 2 (Cell Signaling Technology). Images were acquired with equal exposure times for each channel set. 16bit data was used for quantification of intensity levels of the two stains (see text for sample images compressed to 8 bit).) (B) Example FRAP recovery curves for GFP-myosin IIB at the cortex of ECs embedded in collagen/PA/glass sandwich gels, comparing observed data with fits to biexponential curves. “soft”= 300Pa, “stiff”= 14kPa.

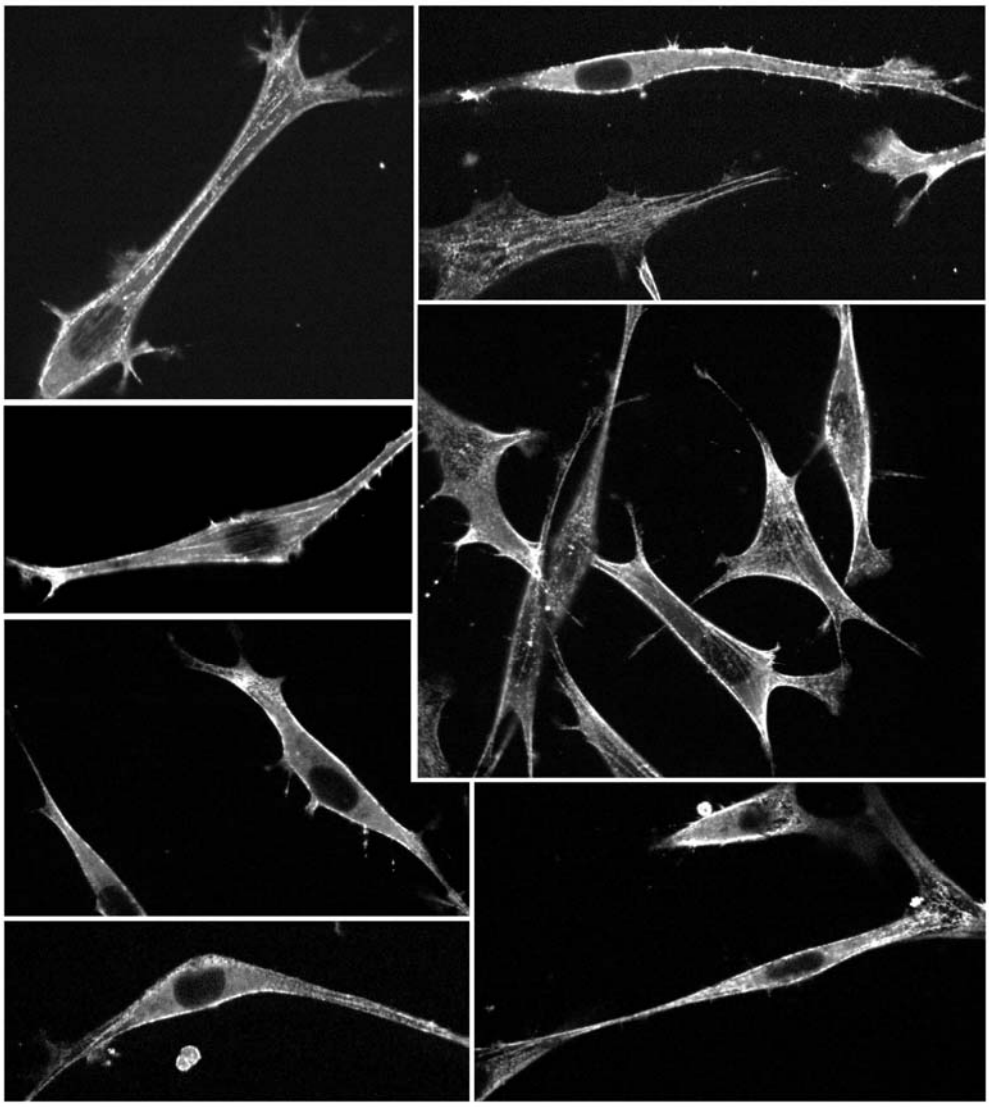

Figure S6. Sample GFP-myosin IIB images. ECs derived from GFP-myosinIIB mice cultured in 3D collagen gels. Cells were imaged live using a spinning disk confocal as described in Methods. Note that GFP-myosinIIB is localized in punctae along bundles, at the cell cortex, and in web-like arrays of punctae behind lamellipodia. Single confocal optical sections shown.

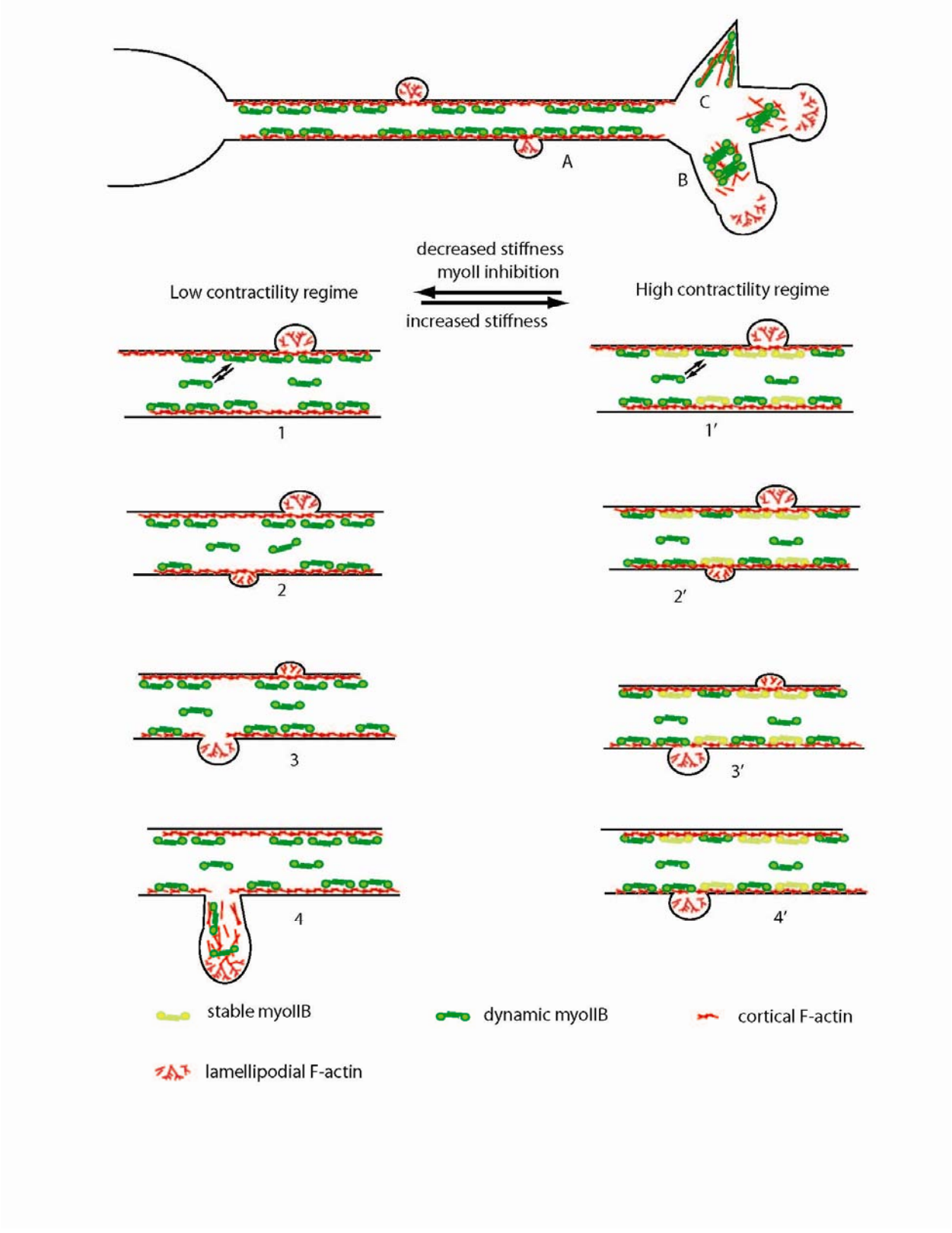
C
A
B
decreased stiffness
myoII inhibition
increased stiffness
Low contractility regime
High contractility regime
1
1′
2
2′
3
3′
4
4′
stable myoIIB
dynamic myoIIB
cortical F-actin
lamellipodial F-actin

Figure S7. Model of myosin II regulation of EC pseudopodial branching. Myosin II is associated and enriched in multiple F-actin containing structures in ECs in 3D. It is predominantly observed at the cell cortex where it forms longitudinal bundles (A), but is also observed in dynamic webs, likely arrays of minifilament "ribbons," [26] behind lamellipodia within advancing pseudopodia(B), and is transiently enriched in retracting pseudopodia (C). When ECs are exposed to migratory stimuli (such as VEGF), transient lamellipodia extend at various points along the cell body or primary pseudopodium. Under conditions of low ECM stiffness/decreased cell contractility, a greater proportion of myosin II dissociates from the EC cortex, which allows for transient local depletions of myosin II from the cell cortex (1, 2). When these transient local depletions coincide with sites of nascent lamellipodia, pseudopod initiation can occur (3,4), as the pulling force of the lamellipodia interacting with the local ECM can allow the pseudopod to "escape" the cortical tension provided by myosin II that usually acts to retract the cortex. Under conditions of higher myosin II activity, or increased ECM stiffness, a greater proportion of myosin II is stably bound at the cell cortex (1', 2'). This maintains consistent cortical contractility, thus reducing local weakening, thereby making lateral lamellipodia unable to escape the cortical tension to form branches (3',4').

Table S1.

Statistical analyses of data, showing n (number of cells or individual protrusions measured), as well as P values and F/Fcrit ratios of data pairs determined by single factor ANOVA analyses. Note that not all possible combinations are shown, only those results discussed in the text.

P-value (F/Fcrit ratio)

	n	in vivo - protrusion	in vivo - retraction	3D col gel (control) protrusion	3D col gel (control) retraction	3D col gel (control) initiations	3D col gel (control) cell speed	3D col gel (control) persistence	3D collagen gel (bleb) protrusion	3D collagen gel (bleb) retraction	3D collagen gel (bleb) cell speed	3D collagen gel (bleb) persistence	3D collagen gel (Y-27632) protrusion	3D collagen gel (Y-27632) retraction	3D collagen gel (Y-27632) initiations	3D collagen gel (Y-27632) cell speed	3D collagen gel (Y-27632) peristence	sandwich gel (soft) protrusion	sandwich gel (soft) retraction	sandwich gel (soft) initiations	sandwich gel (soft) branch points	sandwich gel (stiff) initiations	sandwich gel (stiff) branch points	2D soft branch points	2D stiff branch points	FRAP soft	FRAP stiff
in vivo - protrusion	409	X																									
in vivo - retraction	138		X																								
3D col gel (control) protrusion	298	.023(1.05)		X																							
3D col gel (control) retraction	309		0.005 (1.14)		X																						
3D col gel (control) initiations	18					X																					
3D col gel (control) cell speed	21						X																				
3D col gel (control) persistence	21							X																			
3D collagen gel (bleb) protrusion	255	nd	3.4E-10(11.5)						X																		
3D collagen gel (bleb) retraction	544		nd	1.8E-20(27.4)						X																	
3D collagen gel (bleb) cell speed	21			8.5E-11 (18.62)							X																
3D collagen gel (bleb) persistence	21				1.61E-6(7.73)							X															
3D collagen gel (Y-27632) protrusion	81	nd	2.2E-8(6.2)						0.11(0.64)				X														
3D collagen gel (Y-27632) retraction	106		nd	1.1E-13(16.3)					3.75E-33(53.3)					X												
3D collagen gel (Y-27632) initiations	18			6.5E-6(8.4)											X												
3D collagen gel (Y-27632) cell speed	21			9.28E-09 (12.76)					0.00039 (2.28)							X											
3D collagen gel (Y-27632) peristence	21				0.007 (1.95)					4.25E-8(11.14)							X										
sandwich gel (soft) protrusion	222	.1E-4(4.11)	7.3 E-3(2.51)						nd									X									
sandwich gel (soft) retraction	211		0.15 (0.55)	2.25E-11(22.1)						nd									X								
sandwich gel (soft) initiations	18			0.20(0.40)											nd					X							
sandwich gel (soft) branch points	14																				X						
sandwich gel (stiff) initiations	18			nd											nd				9.5E-9(17.2)			X					
sandwich gel (stiff) branch points	21																			4.1E-9(4.62)			X				
2D soft branch points	35																							X			
2D stiff branch points	33																						3.33E-3(1.8)		X		
FRAP soft	17																									X	
FRAP stiff	17																									3.09E-5(5.67)	